A new model of viscous dissipation for an oscillating wave surge converter

Journal of Engineering Mathematics

A new model of viscous dissipation for an oscillating wave surge converter

--Manuscript Draft--

Manuscript Number:	ENGI-D-16-00037R3
Full Title:	A new model of viscous dissipation for an oscillating wave surge converter
Article Type:	Manuscript
Keywords:	Diffraction; Dissipation; OWSC; Resonance; Wave Energy; Wave-Structure Interaction
Corresponding Author:	Cathal Pádraig Cummins, Ph.D. University College Dublin; University of Edinburgh Dublin, IRELAND
Corresponding Author Secondary Information:	
Corresponding Author's Institution:	University College Dublin; University of Edinburgh
Corresponding Author's Secondary Institution:	
First Author:	Cathal Pádraig Cummins, Ph.D.
First Author Secondary Information:	
Order of Authors:	Cathal Pádraig Cummins, Ph.D. Frédéric Dias, Ph.D.
Order of Authors Secondary Information:	
Funding Information:	Science Foundation Ireland (SFI/10/IN.1/I2996) — Prof. Frédéric Dias
Abstract:	A mathematical model of an oscillating wave surge converter is developed to study the effect that viscous dissipation has on the behaviour of the device. Recent theoretical and experimental testing have suggested that the standard treatment of viscous drag (e.g., Morison's equation) may not be suitable when the effects of diffraction dominate the wave torque on the device. In this paper, a new model of viscous dissipation is presented and explored within the framework of linear potential flow theory, and application of Green's theorem yields a hypersingular integral equation for the velocity potential in the fluid domain. The hydrodynamic coefficients in the device's equation of motion are then calculated, and used to examine the effect of dissipation on the device's performance. A Haskind relationship, expressing the link between the scattering- and radiation-potential problems is derived, and its connection to existing Haskind relations is explored. A sensitivity study of the device's power capture to the magnitude of the dissipation present in the system is carried out for a selection of device widths. The results of the sensitivity study are explained with reference to existing experimental and numerical data. A special focus is given to the effects of dissipation on the performance of a device whose pitching motion is tuned to resonate with the incoming waves.
Response to Reviewers:	In order to get the bibliography into the right format for the journal, we needed to create a new .bst file (spbasic-unsrt.bst), so please note this when compiling/proofing.

Noname manuscript No.
(will be inserted by the editor)

A new model of viscous dissipation for an oscillating wave surge converter

C. P. Cummins · F. Dias

Received: date / Accepted: date

Abstract A mathematical model of an oscillating wave surge converter is developed to study the effect that viscous dissipation has on the behaviour of the device. Recent theoretical and experimental testing have suggested that the standard treatment of viscous drag (e.g., Morison's equation) may not be suitable when the effects of diffraction dominate the wave torque on the device. In this paper, a new model of viscous dissipation is presented and explored within the framework of linear potential flow theory, and application of Green's theorem yields a hypersingular integral equation for the velocity potential in the fluid domain. The hydrodynamic coefficients in the device's equation of motion are then calculated, and used to examine the effect of dissipation on the device's performance. A Haskind relationship, expressing the link between the scattering- and radiation-potential problems is derived, and its connection to existing Haskind relations is explored. A sensitivity study of the device's

C. P. Cummins · F. Dias
UCD School of Mathematics and Statistics,
University College Dublin,
Belfield,
Dublin D04 N2E5,
Ireland
Present address: C. P. Cummins
College of Science and Engineering,
University of Edinburgh,
Edinburgh,
EH9 3BF,
United Kingdom
E-mail: cathal.cummins@ed.ac.uk

F. Dias
Centre de Mathématiques et de Leurs Applications (CMLA),
Ecole Normale Supérieure de Cachan,
Centre National de la Recherche Scientifique (CNRS),
Université Paris-Saclay,
94235 Cachan,
France

power capture to the magnitude of the dissipation present in the system is carried out for a selection of device widths. The results of the sensitivity study are explained with reference to existing experimental and numerical data. A special focus is given to the effects of dissipation on the performance of a device whose pitching motion is tuned to resonate with the incoming waves.

Keywords Diffraction · Dissipation · OWSC · Resonance · Wave Energy · Wave-Structure Interaction

1 Introduction

Oscillating wave surge converters (OWSCs) belong to a family of wave energy converters (WECs) known as 'flap-type' WECs [1]. In its simplest form, an OWSC comprises a buoyant flap that is hinged to the seabed, and typically operates in the nearshore environment where its pitching motion couples with the surge component of the incident waves [2]. Historically, it was maintained that a good wave absorber must be a good wave maker; this leads to the notion of a 'point absorber' for which the effects of diffraction are minimal [3]. In contrast, flap-type WECs are diffraction-dominated devices and, consequently, have received much less attention.

Recent theoretical and experimental studies have shown that OWSCs can achieve high levels of power capture in commonly occurring seas [2]. This has prompted researchers to develop new mathematical models of a flap-type OWSC in order to better understand its hydrodynamic behaviour. To date, this has been achieved through the use of numerical and semi-analytical models to examine the hydrodynamic performance of an OWSC in a channel [4], in the open ocean [5], in a small array [6], and more recently in a large but finite array [7, 8, 9].

In each of the semi-analytical models [4, 5, 6, 7, 9], the fluid is deemed to be inviscid, and hence the effects of viscous dissipation are neglected. However, recent experimental wave tank tests and computational fluid dynamics (CFD) simulations have found that flow separation effects occur at the flap's tips [10]. The numerical simulations in [10] are carried out using the commercial CFD package ANSYS Fluent, and a comparison to laboratory tests shows that such an approach can accurately capture local features of the flow, as well as overall body motion. Unfortunately, the time-consuming nature of wave tank testing and CFD simulations prevented a parametric study from being conducted. As a result, the effect of this viscous dissipation on the hydrodynamic performance of an OWSC has yet to be quantified.

One popular alternative to using CFD is to determine the hydrodynamic coefficients in the flap's equation of motion using a boundary element method (BEM), and introduce an additional term representing viscous dissipation, such as a Morison-type drag law [11]. This choice is suitable for bodies with a small characteristic dimension w' compared to the incident wavelength λ', i.e., for small diffraction parameters: $Kl = 2\pi w'/\lambda' \ll 1$ and comparatively large Keulegan-Carpenter numbers $KC = 2\pi A'_I/w' \gg 1$, where A'_I is the amplitude

of the incident wave. There is no strict cutoff for its validity, but as a useful general rule, Morison's equation is applicable when $KC > 6$, and $Kl < 1$ [12]. However, neither of these conditions are satisfied in the current mathematical modelling of flap-type WECs. In the first place, the diffraction parameter of a flap-type WEC is $O(1)$ in typical environmental conditions [10]. Secondly, the linearity assumption relies on $KC \ll 1$, hence the validity of using a Morison-type drag law for flap-type WECs within the framework of linear potential flow theory is questionable.

A lesser-known alternative is to modify the inviscid theory in regions of the fluid domain where the effects of viscous dissipation are non-negligible, e.g., bilge keels, or sharp edges of hull elements [13]. In this way, the effects of viscous dissipation are confined to the region around the flap's tips, where they are known to occur [10]. This modelling approach is adopted in [13] to eliminate the unphysical spikes in the resonant free-surface of a moonpool that are predicted by inviscid potential flow theory. In order to include the effects of vortex shedding, the authors first extend a control surface from the moonpool's sharp edge down to the seabed, and then impose a pressure discharge across this control surface. The pressure discharge law used in [13] assumes a functional relationship between the pressure drop and the local flow velocity, which characterises the effects of dissipation. The authors find excellent agreement with model tests, concluding that such a methodology is an accurate and efficient way to incorporate the effects of vortex shedding into the inviscid theory.

Treating the dissipative effects of viscosity as equivalent losses in pressure is not a new idea: the same modelling approach is used in the study of wave transmission through porous screens and breakwaters. Typically, such screens are used to damp out the sloshing motion in wave tanks or to act as tuned liquid dampers in order to absorb unwanted vibrations [14]. Numerous models have been put forward for this pressure loss law, which assume that the pressure loss is a function of the local flow velocity as in [13] above. In [15], the oscillatory flow through a porous screen is examined. It is suggested that the dissipative and inertial effects due to the screen should be modelled using a functional relationship between the pressure drop and the flow velocity. In [16], the oscillatory flow through a number of thin porous screens in a narrow wave tank is considered using the same model as in [15] to account for the dissipative and inertial effects due to the presence of the screen. In [17], the diffraction of water waves from a thin porous breakwater is studied. The authors derive a boundary condition for the loss in pressure across the breakwater.

The pressure discharge law typically takes the form of a linear [15, 17, 13] or quadratic [18] function of the local flow velocity. In addition, we can use an effective linear law in place of the nonlinear one using, say, the Lorentz principle of equivalent work [19, 20]. Indeed, previous numerical models of OWSCs have used effective linear [21, 11] and quasi-linear [22] drag laws in place of the standard Morison (quadratic) drag law [11]. In each of [15, 16, 17, 13], it is assumed that the pressure drop across the screen/breakwater due to viscous effects is a linear function of the local flow velocity. The complex-valued

parameter, which characterises the inertial and viscous effects, is treated as an empirical quantity. In [17], this parameter is termed the 'porous-wall-effect-parameter' G and is determined by comparison to model tests [23].

In this paper, we assess the effect that viscous dissipation has on an OWSC by modifying the semi-analytical theory of [4] to include the effects of viscous dissipation near the flap's edge. We achieve this by applying an effective pressure discharge in the vicinity of the flap's tips [13]. Formulating the problem in this way yields a hypersingular integral equation for the fluid's velocity potential, the solution to which is obtained in terms of a series of Chebyshev polynomials of the second kind. The equation of motion of the flap is then solved in the frequency domain, and the solution is used to conduct a parametric analysis of an OWSC for a variety of environmental conditions and device dimensions. The effect of viscous dissipation on the device's performance is then quantified. We do not conduct dedicated model tests to validate our model, but rather our results may be compared to model tests in a straightforward way [23, 13].

The paper is organised as follows: in Sect. 2, the mathematical model is formulated, non-dimensionalised, and the solution is achieved through an application of Green's theorem (as set out in the Appendix). The hydrodynamic coefficients in the device's equation of motion are found and in turn this equation of motion is solved in the frequency domain. In Sect. 3, a sensitivity study of the effect that viscous dissipation has on the device's performance is conducted. Within the framework of this sensitivity study, the influence of the device's dimensions on the device's performance is quantified, and it is shown that the sensitivity of the device's performance to dissipation depends strongly on the diffraction parameter Kl. Sect. 3 concludes with a special focus on the effect that dissipation has on the flap's resonant hydrodynamic behaviour. Finally, the connection between the current findings and previous experimental and theoretical results is explored in Sect. 4 and Sect. 5.

2 Mathematical model

Consider an OWSC in an open ocean of constant water depth h', where the prime indicates a quantity with a physical dimension. The OWSC is represented as a buoyant box-shaped flap of width w' and thickness $2a'$, hinged at a depth d' on a rigid platform of height $h'-d'$ as shown in figure 1. Monochromatic waves of amplitude A'_I and period T' (see figure 2) are normally incident upon the flap, which set the device oscillating about its hinge line.

Let $\theta'(t')$ be the pitching amplitude of the device, which is positive if the flap's rotation is counterclockwise, and let t' denote time. We define the reference system of coordinates $O'(x', y', z')$ with x' pointing in the opposite direction to the incoming waves, and let the y'-axis lie along the width of the device and the z'-axis points upwards from the still water level. The origin O' is located in the center of the device at the still water level.

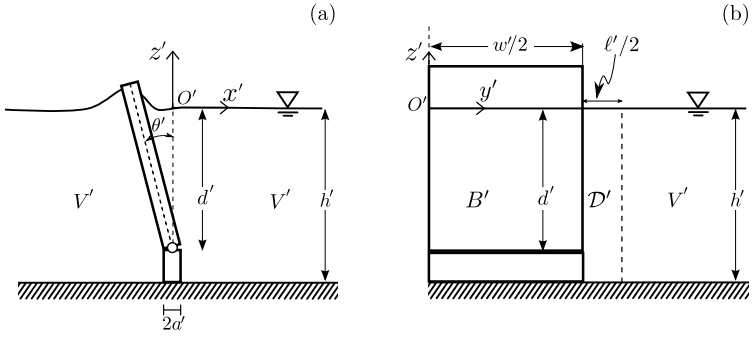

Fig. 1 The geometry of the surface-piercing OWSC with dissipative surface $\mathcal{D}'$ [13] extending from the fluid's free surface to the seabed: (a) side (b) front view.

The fluid is deemed to be inviscid and incompressible, and the flow irrotational. Hence, there exists a potential $\Phi'(x', y', z', t')$ for the velocity field $\boldsymbol{v}' = \nabla'\Phi'$ that satisfies Laplace's equation

$$\nabla'^2\Phi' = 0, \quad (x', y', z') \in V', \tag{1}$$

in the fluid domain V'. We further assume that the incident wave amplitude is small compared to the width of the device: $A'_I \ll w'$. As a consequence, the angular rotation of the flap induced by the incoming waves is small and the behaviour of the system is linear [4]. At the free surface, the linearised kinematic-dynamic boundary condition leads to

$$\Phi'_{,t't'} + g\Phi'_{,z'} = 0, \quad z' = 0, \tag{2}$$

with g the acceleration due to gravity and a subscripted comma indicating differentiation. We require zero flux of the fluid through the seabed

$$\Phi'_{,z'} = 0, \quad z' = -h'. \tag{3}$$

On the flap we have the kinematic condition

$$\Phi'_{,x'} = -\theta'_{,t'}(t')(z' + d')\mathrm{H}(z' + d'), \quad x' = \pm 0, \quad |y'| < w'/2, \tag{4}$$

where H stands for the Heaviside step function and where we have applied the thin-body approximation

$$2a' \ll w'. \tag{5}$$

As is typical in problems such as these, we will split the velocity potential into an incident, diffracted, and radiated part as follows:

$$\Phi' = \Phi^{I\prime} + \Phi^{D\prime} + \Phi^{R\prime}. \tag{6}$$

We will further require that the wave field generated by the interaction between the incoming waves and the flap (i.e., the diffracted and radiated parts of the wave field) must be outgoing at large distances $r' = \sqrt{x'^2 + y'^2}$ from the flap [6].

Recent laboratory tests and numerical simulations have confirmed that vortices are generated and shed from the tips of the flap at each half wave period [10]. Hence, to incorporate the dissipative effects due to viscosity, we introduce a so-called 'dissipative surface' $\mathcal{D}'$ close to the flap's edge, which occupies the region $\frac{1}{2}w' < |y'| < \frac{1}{2}(w' + \ell')$ as shown in figure 1(b) and figure 2. We supplement equations (1)-(4) with the additional boundary condition on $\mathcal{D}'$. Across $\mathcal{D}'$, we impose a pressure discharge $\Delta P'$, which we assume to be a function of the local velocity component ($v'_n = \Phi'_{,n}$) along the outward unit normal vector $\boldsymbol{n}$ to $\mathcal{D}'$ in the wave direction

$$\Delta P' = f\left(\Phi'_{,n}\right). \tag{7}$$

The relationship (7) represents the energy loss due to internal fluid dissipation near the flap's edge [16, 17, 13] – here

$$\Delta P'(y', z', t') = P'(-0, y', z', t') - P'(+0, y', z', t'), \tag{8}$$

denotes the difference in the pressure P' from the left to the right side of the flap/dissipative surface in the wave direction. In the rest of the paper, we will use the Δ notation exclusively to represent jumps in hydrodynamic quantities. In addition to (7), we require continuity of the velocity field between the left and right faces of $\mathcal{D}'$.

Pressure discharge laws such as (7) are common in the literature, with the function f typically taking the form of a linear [15, 17, 13] or quadratic [18] function of the local flow velocity. Following previous studies [21, 11, 13], let us consider a linear form of f; this leads to the following boundary condition:

$$\Delta\Phi^{(R,D)\prime}(y', z', t') = -\frac{\mathrm{i}\bar{\epsilon}g}{\omega'^2}\Phi^{(R,D)\prime}_{,x'}(\pm 0, y', z', t'), \quad w'/2 < |y'| < (w' + \ell')/2, \tag{9}$$

where $\mathrm{i} = \sqrt{-1}$, $\omega' = 2\pi/T'$ is the wave's angular frequency, and the dimensionless parameter $\bar{\epsilon}$ is a measure of the amount of dissipation present in the system and is termed the 'dissipative-effect parameter'. In this paper, $\bar{\epsilon}$ is treated as an empirical quantity that may be determined through dedicated laboratory tests [16, 23, 13]. The lateral extent of the dissipative surface ℓ' in (9) is chosen to reflect the characteristic size of the vortices shed from the edges of the flap as observed in laboratory tests [10].

We remark in passing that $\bar{\epsilon}$ is related in a straightforward way to its porous-media counterpart, the 'porous-wall-effect-parameter' G [17], through the relationship

$$\bar{\epsilon} = \frac{\tanh k'h'}{\Re\{G\}}. \tag{10}$$

The numerator in (10) is typically between 0.5 and 1, so the overall magnitude of $\bar{\epsilon}$ is determined by the reciprocal of $\Re\{G\}$. Note here that $\Im\{\bar{\epsilon}\} = 0$: in terms of porous media flows, this would indicate that the inertial forces due to the presence of the control surface are negligible compared to the resistive forces.

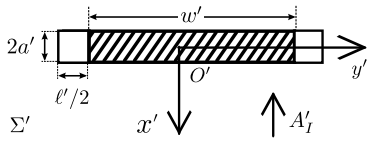

Fig. 2 Top view of the surface-piercing OWSC with the dissipative volume extended from the flap's tips, and incident waves of amplitude A'_I travelling in the direction of $-x'$.

Continuity of the fluid's velocity across $\mathcal{D}'$ yields

$$\Delta\Phi^{(R,D)\prime}_{,x'}(y',z',t') = 0, \quad w'/2 < |y'| < (w'+\ell')/2, \tag{11}$$

where, in the same way as in (8),

$$\Delta\Phi^{(R,D)\prime}(y',z',t') = \Phi^{(R,D)\prime}(-0,y',z',t') - \Phi^{(R,D)\prime}(+0,y',z',t'), \tag{12}$$

denotes the difference in the diffraction/radiation potentials from the left to the right side of the flap/dissipative surface in the wave direction, and likewise

$$\Delta\Phi^{(R,D)\prime}_{,x'}(y',z',t') = \Phi^{(R,D)\prime}_{,x'}(-0,y',z',t') - \Phi^{(R,D)\prime}_{,x'}(+0,y',z',t'), \tag{13}$$

denotes the difference in the x'-component of the velocity from the left to the right side of the flap/dissipative surface in the wave direction.

2.0.1 Non-dimensionalisation

Let A' denote the amplitude scale of the wave field (in which the incident waves have amplitude A'_I) and introduce the following dimensionless variables:

$$\left.\begin{aligned} &(x,y,z,r) = (x',y',z',r')/w', \quad t = \sqrt{g/w'}t', \quad \Phi = \left(\sqrt{gw'}A'\right)^{-1}\Phi', \\ &\omega = \omega'\sqrt{w'/g}, \quad \theta = (w'/A')\theta', \end{aligned}\right\} \tag{14}$$

and the dimensionless constants

$$(h,d,\ell) = (h',d',\ell')/w', \quad A_I = A'_I/A'. \tag{15a,b}$$

To ensure that the flap performs linear motion, we require that $A'_I \ll w'$. Further, let the dimensionless potential Φ comprise the dimensionless incident, diffraction, and radiation potentials as follows:

$$\Phi = \Phi^I + \Phi^D + \Phi^R. \tag{16}$$

2.1 Semi-analytical solution

We may separate the time dependence out of the problem as follows:

$$\theta(t) = \Re\left\{\Theta \mathrm{e}^{-\mathrm{i}\omega t}\right\}, \quad \Phi(x,y,z,t) = \Re\left\{\phi(x,y,z)\mathrm{e}^{-\mathrm{i}\omega t}\right\}, \tag{17a,b}$$

where the complex velocity potential ϕ comprises contributions from the incident, diffraction, and radiation problems

$$\phi(x,y,z) = \phi^I(x,z) + \phi^D(x,y,z) + \mathcal{V}\phi^R(x,y,z), \tag{18}$$

and the complex incident potential ϕ^I is given by

$$\phi^I = -\frac{\mathrm{i}A_I}{\omega}\frac{\cosh k(z+h)}{\cosh kh}\mathrm{e}^{-\mathrm{i}kx}; \tag{19}$$

here, k is the wavenumber satisfying the dimensionless dispersion relation

$$\omega^2 = k\tanh kh, \tag{20}$$

$\mathcal{V} = \mathrm{i}\omega\Theta$ is the complex angular velocity of the flap, and Θ is the complex pitching amplitude made by the flap, which is found as part of the solution. In (17), we have implied that there is just a single radiation problem since we keep the dissipative surfaces fixed.

We nondimensionalise the governing equations according to (14) and (15). We then substitute the decompositions (17) and (18) into (1)-(4), (9), and (11), which yields the following equations:

$$\nabla^2\phi^{(R,D)} = 0, \quad (x,y,z) \in V, \tag{21}$$

in the fluid domain

$$\phi^{(R,D)}_{,z} - \omega^2\phi^{(R,D)} = 0, \quad z = 0, \tag{22}$$

at the free surface

$$\phi^{(R,D)}_{,z} = 0, \quad z = -h, \tag{23}$$

at the seabed. On the flap, we find

$$\begin{Bmatrix}\phi^R_{,x}\\ \phi^D_{,x}\end{Bmatrix} = \begin{Bmatrix}(z+d)\mathrm{H}(z+d)\\ -\phi^I_{,x}\end{Bmatrix}, \quad x = \pm 0, \quad |y| < 1/2. \tag{24}$$

Across the dissipative surface, we have

$$\phi^{(R,D)}_{,x} = -\frac{\omega^2}{\mathrm{i}\bar{\epsilon}}\Delta\phi^{(R,D)}, \quad x = \pm 0, \quad 1/2 < |y| < (1+\ell)/2, \tag{25}$$

and continuity of velocity

$$\Delta\phi^{(R,D)}_{,x} = 0, \quad 1/2 < |y| < (1+\ell)/2. \tag{26}$$

Following previous authors [5], we separate out the vertical dependence of the solution as follows:

$$\phi^{(R,D)}(x,y,z) = \sum_{n=0}^{\infty} \varphi_n^{(R,D)}(x,y) Z_n(z), \tag{27}$$

where $Z_n(z)$ are the well-known normalised vertical eigenmodes of the flat-bottom water wave problem

$$Z_n(z) = \frac{\sqrt{2}\cosh\kappa_n(z+h)}{\left(h + \omega^{-2}\sinh^2\kappa_n h\right)^{1/2}}, \quad n = 0, 1, \ldots, \tag{28}$$

which satisfy the orthogonality relation

$$\int_{-h}^{0} Z_n(z) Z_m(z) \mathrm{d}z = \delta_{nm}, \tag{29}$$

with $n \in \mathbb{N}_0$, $m \in \mathbb{N}$, δ_{nm} the Kronecker delta, and κ_n defined as

$$\kappa_0 = k, \quad \kappa_n = \mathrm{i}k_n, \quad n = 1, 2, \ldots, \tag{30}$$

where k and k_n are the positive solutions to the dispersion relations (20) and

$$\omega^2 = -k_n \tan k_n h, \quad n = 1, 2, \ldots, \tag{31}$$

respectively.

By inserting (27) into the governing equations (21)-(26), we obtain the Helmholtz equation

$$\left(\nabla^2 + \kappa_n^2\right) \varphi_n^{(R,D)}(x,y) = 0, \quad (x,y) \in \Sigma, \tag{32}$$

in the reduced 2D fluid domain Σ (see figure 2), and boundary conditions

$$\sum_{n=0}^{\infty} Z_n(z) \begin{Bmatrix} \varphi_{n,x}^R \\ \varphi_{n,x}^D \end{Bmatrix} (x,y) = \begin{Bmatrix} (z+d)\mathrm{H}(z+d) \\ -\phi_{,x}^I \end{Bmatrix}, \quad x = \pm 0, \quad |y| < 1/2, \tag{33}$$

on the flap, and on the dissipative surface we find

$$\sum_{n=0}^{\infty} \varphi_{n,x}^{(R,D)}(x,y) Z_n(z) = -\frac{\omega^2}{\mathrm{i}\bar{\epsilon}} \sum_{n=0}^{\infty} \Delta\varphi_n^{(R,D)}(y) Z_n(z), \quad x = \pm 0, \quad 1/2 < |y| < (1+\ell)/2, \tag{34}$$

and continuity of the fluid's velocity across $\mathcal{D}$ yields

$$\sum_{n=0}^{\infty} \Delta\varphi_{n,x}^{(R,D)}(y) Z_n(z) = 0, \quad 1/2 < |y| < (1+\ell)/2. \tag{35}$$

We may further simplify (33)-(35) by multiplying both sides of each equation by $Z_m(z)$ and integrating over the entire water column; using the orthogonality relation (29), we find

$$\begin{Bmatrix} \varphi^R_{n,x} \\ \varphi^D_{n,x} \end{Bmatrix}(x,y) = \begin{Bmatrix} f_n \\ A_I q_n \end{Bmatrix}, \quad x = \pm 0, \quad |y| < 1/2, \tag{36}$$

where the real quantities q_n and f_n are defined as

$$q_n = \frac{k\left(h + \omega^{-2}\sinh^2 kh\right)^{1/2}}{\sqrt{2}\omega\cosh kh}\delta_{n0}, \tag{37}$$

and

$$f_n = \frac{\sqrt{2}\left[d\kappa_n \sinh\kappa_n h + \cosh\kappa_n(h-d) - \cosh\kappa_n h\right]}{\kappa_n^2\left(h + \omega^{-2}\sinh^2\kappa_n h\right)^{1/2}}. \tag{38}$$

On the dissipative surface, we find

$$\varphi^{(R,D)}_{n,x}(\pm 0, y) = -\frac{\omega^2}{\mathrm{i}\bar{\epsilon}}\Delta\varphi^{(R,D)}_n(y), \quad 1/2 < |y| < (1+\ell)/2, \tag{39}$$

and continuity of the fluid's velocity across $\mathcal{D}$ yields

$$\Delta\varphi^{(R,D)}_{n,x}(y) = 0, \quad 1/2 < |y| < (1+\ell)/2. \tag{40}$$

The solution to equations (32), (36), (39), and (40) is found by application of Green's theorem to $\varphi^{(R,D)}_{n,x}$ and G_n (see Appendix) in a large circumference enclosing all regions of the reduced 2D fluid domain Σ. This yields a hypersingular equation for the diffraction and radiation problems, as outlined in the Appendix. To resolve this singularity, the solutions to the diffraction and radiation problems are represented in terms of a series of Chebyshev polynomials of the second kind; the complex diffraction potential ϕ^D reads

$$\begin{aligned}\phi^D(x,y,z) = -\frac{\mathrm{i}A_I}{8}kxZ_0(z)\sum_{m=1}^{3} w_m \sum_{p=0}^{p_{\max}} a_{0mp}\int_{-1}^{1}(1-\zeta^2)^{1/2}U_p(\zeta) \\ \times \frac{H_1^{(1)}\left(k\sqrt{x^2 + \left(y - \left(w_m\zeta + u_m\right)/2\right)^2}\right)}{\sqrt{x^2 + \left(y - \left(w_m\zeta + u_m\right)/2\right)^2}}\mathrm{d}\zeta,\end{aligned} \tag{41}$$

where w_m and u_m are defined in the Appendix. In (41), $H_1^{(1)}$ is the outgoing Hankel function of the first kind and first order, U_p is the Chebyshev polynomial of the second kind and order $p \in \mathbb{N}_0$, and the complex coefficients a_{0mp} assume values that ensure that the diffraction potential ϕ^D satisfies the no-flux condition on the flap (lower line of (24)) and the pressure discharge and continuity conditions on the dissipative surfaces (25) and (26) respectively. These coefficients are computed by solving a system of linear equations using

a collocation scheme – see Appendix. In the same way, the complex radiation potential ϕ^R is given by

$$\phi^R(x,y,z) = -\frac{\mathrm{i}}{8}\sum_{n=0}^{n_{\max}} \kappa_n x Z_n(z) \sum_{m=1}^{3} w_m \sum_{p=0}^{p_{\max}} b_{nmp} \int_{-1}^{1} (1-\zeta^2)^{1/2} U_p(\zeta) \times \frac{H_1^{(1)}\left(\kappa_n \sqrt{x^2 + \left(y - \left(w_m\zeta + u_m\right)/2\right)^2}\right)}{\sqrt{x^2 + \left(y - \left(w_m\zeta + u_m\right)/2\right)^2}} \mathrm{d}\zeta. \quad (42)$$

In (42), the complex coefficients b_{nmp} ensure that the radiation potential satisfies the kinematic condition on the flap (upper line of (24)) and the pressure discharge and continuity conditions on the dissipative surfaces (25) and (26) respectively. Note that in order to compute these coefficients in the expressions for ϕ^D and ϕ^R, the series in n and p are truncated at finite values $n_{\max}$ and $p_{\max}$ respectively.

2.2 Body motion and wave power absorption

To solve the problem fully, we must determine the pitching amplitudes in $(17a)$. To do this, we solve the equation of motion for the flap in the frequency domain:

$$\left[-\omega^2\left(I+\mu\right) + C - \mathrm{i}\omega\left(\nu + \nu_{\mathrm{pto}}\right)\right]\Theta = F, \quad (43)$$

where $I = I'/(\rho w'^5)$, $C = C'/(\rho g w'^4)$, and $\nu_{\mathrm{pto}} = \nu'_{\mathrm{pto}}/(\rho w'^4\sqrt{gw'})$ are respectively the dimensionless moment of inertia, buoyancy torque, and the power take off (PTO) damping of the flap. The hydrodynamic coefficients in (43) are the dimensionless complex exciting torque

$$F = -\frac{\mathrm{i}\pi\omega}{4} A_I w_2 f_0 a_{020}, \quad (44)$$

from the diffraction problem, the dimensionless added mass

$$\mu = \frac{\pi w_2}{4}\Re\left\{\sum_{n=0}^{\infty} f_n b_{n20}\right\}, \quad (45)$$

and dimensionless added damping

$$\nu = \frac{\pi\omega w_2}{4}\Im\left\{\sum_{n=0}^{\infty} f_n b_{n20}\right\}, \quad (46)$$

from the radiation problems. The equation (43) and coefficients (44)-(46), have been derived in [5] for an arbitrary number of flaps without dissipation, leading to as many equations as there are flaps. In our case, we consider the equations/coefficients for a 3-flap system but since the dissipative surfaces remain fixed, we have just a single equation of motion.

Table 1 Physical dimensions of the OWSC, the wave conditions considered, and the width of the dissipative regions.

w'(m)	h' (m)	A_I' (m)	d' (m)	ℓ' (m)
$\{12, 18, 26\}$	10.9	0.3	9.4	1.8

The absorbed power $\mathcal{P}$ over a cycle is calculated using the formula [4]

$$\mathcal{P} = \frac{1}{2}\omega^2 \nu_{\text{pto}} \frac{|F|^2}{\left|C - \omega^2 (I + \mu) - \mathrm{i}\omega (\nu + \nu_{\text{pto}})\right|^2}. \tag{47}$$

Following previous authors [4], the extracted power (47) can be optimised by adjusting the PTO damping $\nu_{\text{pto}} = \nu_{\text{pto}}(\omega)$ so that $\partial\mathcal{P}/\partial\nu_{\text{pto}} = 0$. This leads to the following expression for the optimal PTO damping

$$\nu_{\text{pto}}(\omega) = \sqrt{\nu^2 + \frac{\left[C - \omega^2 (I + \mu)\right]^2}{\omega^2}}, \tag{48}$$

and inserting this back into (47) yields the following expression for the power generated:

$$\mathcal{P} = \frac{1}{4} \frac{|F|^2}{(\nu_{\text{pto}} + \nu)}. \tag{49}$$

In practice, one might need to select a fixed PTO damping for the device, but this case is not examined in this paper. Instead, we will always select our optimal PTO damping according to (48); in (49) and in the rest of the paper, the dependence of the optimal PTO damping on ω is implied. To assess the performance of the OWSC, the capture factor, which is defined as the ratio of the power output of the device to the power of the incident wave per unit width of the device

$$C_F = \frac{|F|^2}{2A_I^2 C_g (\nu_{\text{pto}} + \nu)}, \tag{50}$$

is computed. In (50),

$$C_g = \frac{\omega}{2k}\left(1 + \frac{2kh}{\sinh 2kh}\right) \tag{51}$$

is the group velocity of the incident wave in dimensionless variables. The expressions for the power (49) and capture factor (50), when written in this form, make it clear that the device's power capture and performance are dominated by the exciting torque [1]. There are other expressions for WEC performance in the literature: in [24], the authors characterise the absorptive properties of a WEC with reference only to the radiated wave at large distances from the device. Such an expression is particularly useful for a point absorber WEC, whose performance relies on its ability to radiate waves.

To assess the OWSC's performance with regard to increasing dissipation levels, we consider an OWSC with physical dimensions and environmental

conditions the same as those that were used in previous studies (see table 1) [5]. We examine the effect that changing the flap's width has on power capture with reference to varying the dissipation-effect parameter. Note that, although we make the simplifying assumption that the flap is thin, this does not affect the buoyancy torque, which is calculated using the submerged volume of the flap. In the same way, the width of the dissipative region is selected to be of the same order of magnitude as a typical flap's thickness, as this is the region in which we expect the effects due to viscous losses to be confined [10]. The value of ℓ' appears in table 1, and is kept fixed throughout the parametric analysis.

2.3 Behaviour in the far field

To assess our results, let us consider the following integral I_{nmp} appearing in the expressions (41) and (42) for the complex velocity potentials $\phi^{(R,D)}$:

$$I_{nmp} = \int_{-1}^{1} (1-\zeta^2)^{1/2} U_p(\zeta) \frac{H_1^{(1)}\left(\kappa_n \sqrt{x^2 + (y - (w_m\zeta + u_m)/2)^2}\right)}{\sqrt{x^2 + (y - (w_m\zeta + u_m)/2)^2}} \mathrm{d}\zeta. \quad (52)$$

We wish to examine the behaviour of I_{nmp} in the far field. Since the evanescent modes ($n > 0$) decay exponentially quickly far from the device [5], let us consider only the propagative $n = 0$ mode of (52), and expressing the Cartesian coordinates (x, y) in terms of plane polar coordinates (r, γ) as follows:

$$(x, y) = r(\cos\gamma, \sin\gamma), \quad (53)$$

then we find

$$I_{0mp} = \int_{-1}^{1} (1-\zeta^2)^{1/2} U_p(\zeta) \frac{H_1^{(1)}\left(kr \sqrt{1 + [(w_m\zeta + u_m)/2r]^2}\right)}{r\sqrt{1 + [(w_m\zeta + u_m)/2r]^2}} \mathrm{d}\zeta. \quad (54)$$

To examine the behaviour of I_{0mp} in the far field, consider the large-r asymptotic behaviour of $H_1^{(1)}$ (see equation (37) in [5]). Carrying out the algebra gives the following large-r asymptotic behaviour of the complex velocity potentials:

$$\begin{Bmatrix} \phi^R \\ \phi^D \end{Bmatrix} (r, \gamma, z) = -xZ_0(z) \frac{\mathrm{i}k\pi}{16r} \sqrt{\frac{2}{\pi kr}} \mathrm{e}^{\mathrm{i}(kr - 3\pi/4)} \cos\gamma \sum_{m=1}^{3} w_m \begin{Bmatrix} b_{0m0} \\ A_I a_{0m0} \end{Bmatrix}. \quad (55)$$

Taking each potential in turn, the diffraction potential (bottom line of (55)) reads

$$\phi^D(r, \gamma, z) = -\frac{\mathrm{i}A_I}{\omega} \mathcal{A}^D(\gamma) \frac{\cosh k(z+h)}{\cosh kh} \sqrt{\frac{2}{\pi kr}} \mathrm{e}^{\mathrm{i}(kr - \pi/4)}, \quad (56)$$

where $\mathcal{A}^D(\gamma)$, defined as

$$\mathcal{A}^D(\gamma) = -\frac{\mathrm{i}\pi}{8\sqrt{2}} k\cos\gamma \sum_{m=1}^{3} w_m a_{0m0} \frac{\omega\cosh kh}{\left(h+\omega^{-2}\sinh^2 kh\right)^{1/2}}, \tag{57}$$

is the angular variation of the diffracted wave. In the same way, the radiation potential in the far field may be written as

$$\phi^R(r,\gamma,z) = -\frac{\mathrm{i}}{\omega}\mathcal{A}^R(\gamma)\frac{\cosh k(z+h)}{\cosh kh}\sqrt{\frac{2}{\pi kr}}\mathrm{e}^{\mathrm{i}(kr-\pi/4)}, \tag{58}$$

where $\mathcal{A}^R(\gamma)$, defined as

$$\mathcal{A}^R(\gamma) = -\frac{\mathrm{i}\pi}{8\sqrt{2}} k\cos\gamma \sum_{m=1}^{3} w_m b_{0m0} \frac{\omega\cosh kh}{\left(h+\omega^{-2}\sinh^2 kh\right)^{1/2}}, \tag{59}$$

is the angular dependence of the radially spreading radiated wave. Now consider the propagative mode of the radiation damping

$$\nu_{\mathrm{prop}} = \frac{\pi w_2\omega}{4}\mathrm{Im}\left\{f_0 b_{020}\right\}, \tag{60}$$

where we have omitted the higher order eigenmodes in (46) as they remain trapped to the body [5]. Using (59), we may express $w_2 b_{020}$ in terms of $\mathcal{A}^R(0)$, which yields the following expression:

$$w_2 b_{020} = \frac{4\mathrm{i}}{\pi\omega}\frac{2\sqrt{2}\mathcal{A}^R(0)}{k\cosh kh}\left(h+\omega^{-2}\sinh^2 kh\right)^{1/2} - w_1\left(b_{010}+b_{030}\right). \tag{61}$$

Inserting this into (60) yields

$$\nu_{\mathrm{prop}} = \frac{\pi\omega}{4} f_0 \Im\left\{\frac{8\mathrm{i}\sqrt{2}\mathcal{A}^R(0)}{\pi\omega k\cosh kh}\left(h+\omega^{-2}\sinh^2 kh\right)^{1/2} - \frac{\ell}{2}\left(b_{010}+b_{030}\right)\right\}. \tag{62}$$

It can be shown that the two linear systems of equations for the radiation and diffraction problems have identical coefficient matrices, and hence our problem yields the following solvability condition:

$$b_{020}q_0 = a_{020}f_0, \tag{63}$$

to ensure uniqueness of the solution [4]. We may, therefore, express the exciting torque (44) in terms of the coefficients of the radiation problem

$$F = -\frac{\mathrm{i}\pi}{4} A_I w_2 \omega q_0 b_{020}, \tag{64}$$

and using (61), we may express the complex exciting torque in terms of $\mathcal{A}^R(0)$ as follows:

$$F = \frac{4}{k} A_I C_g \mathcal{A}^R(0) + \frac{\mathrm{i}\pi}{4}\frac{\ell}{2} A_I \omega q_0 \left(b_{010}+b_{030}\right). \tag{65}$$

Combining (62) and (65), we may express ν_{prop} in terms of F

$$\nu_{\text{prop}} = \left(d + \frac{\cosh(k(h-d)) - \cosh kh}{k \sinh kh} \right) \text{Re} \left\{ \frac{F}{A_I} \right\} \frac{\tanh kh}{kC_g}. \tag{66}$$

Interestingly, (66) is identical to the Haskind relation for an OWSC in an open ocean (or in a channel) without dissipation [4, 5]. Although not a sufficient criteria for numerical accuracy, it is used in this paper as a quick check of the accuracy of the calculations of the numerical scheme, achieving a relative error of $O\left(10^{-15}\right)$ between the left- and right-hand sides of (66) using just the first $P = 5$ terms of the series of Chebyshev polynomials. All results presented in this paper converge to at least the same level of accuracy as previous studies on WEC arrays (see [6]) using the first $P = 7$ Chebyshev polynomials and the first $N = 3$ vertical eigenmodes. In order to achieve a consistent level of accuracy near resonant peaks, however, it was necessary to include the first $P = 13$ Chebyshev polynomials and first $N = 3$ vertical eigenmodes.

3 The results

3.1 Influence of dissipation on power capture

In figures 3 and 4, we examine the effect that increasing the dissipation-effect parameter $\bar{\epsilon}$ has on the hydrodynamic behaviour of the OWSC. In the limit as $\bar{\epsilon} \to 0$, the exciting torque, added mass/damping, and capture factors are identical to that for a single flap in the open ocean without dissipation [5]. Increasing $\bar{\epsilon}$ leads to a decrease in the peak values of all three hydrodynamic coefficients and the capture factor, as can be seen in figure 4. For short-period waves (wave periods smaller than the peak period), the hydrodynamic quantities are insensitive to the value of $\bar{\epsilon}$. The capture factor is found to monotonically decrease with increasing $\bar{\epsilon}$ for all flap dimensions and typical wave conditions.

3.2 Sensitivity to dissipation: the influence of diffraction

To examine the effect that the flap's width has on power capture, we consider the capture factor of flaps with the three different widths given in table 1. In order to investigate how the flap's width affects the power capture's dependence on dissipation, we focus on the peak and trough values of the capture factor curve. In figure 5, we plot the percentage decrease in the peak (figure 5a) and trough (figure 5b) values of C_F against $\bar{\epsilon}$ for the three flap widths considered.

For each flap width considered in this parametric analysis, we find that the peak values of C_F are less sensitive to the magnitude of $\bar{\epsilon}$ than the trough values. In the former, there is about a 1% change in C_F for $\bar{\epsilon}$ taking values between 0 and 0.01; in the latter, the change is 3% over the same range of $\bar{\epsilon}$.

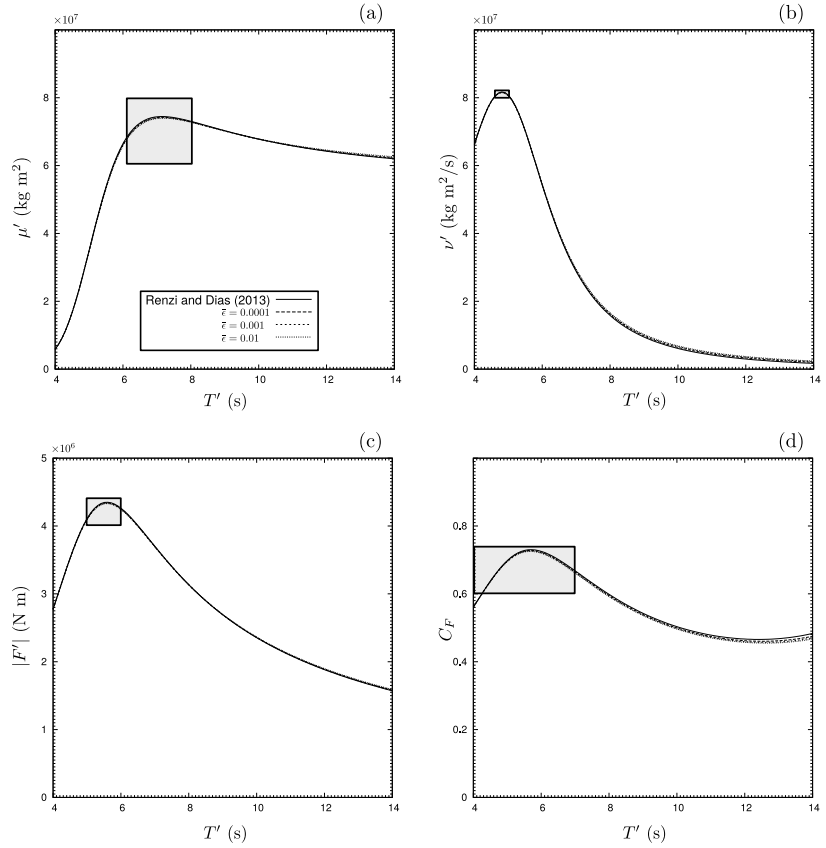

Fig. 3 The dependence of the hydrodynamic coefficients μ', ν', and $|F'|$ in dimensional variables, and the capture factor C_F on the magnitude of the dissipative-effect parameter $\bar{\epsilon}$ as a function of the incident wave period T' in seconds for a flap of width $w' = 18$ m. The grey box that encloses the peak in each of (a)-(d) indicates the extent of the plot region in figure 4.

Furthermore, we find that the sensitivity of C_F to dissipation is affected by the flap's width: the narrower the flap, the more sensitive is its power capture to the value of $\bar{\epsilon}$, and this is especially true at longer wave periods – see figure 5(b).

The connection between existing experimental tank tests/CFD simulation results and the present work is also illustrated in figure 5(b) and figure 6. In the former, we have labelled each of curves from our parametric study with the value of its associated diffraction parameter Kl. Note that the trend in figure 5(b) is present in figure 5(a), but since the diffraction parameters near a peak are larger ($Kl \approx 2.4$), the sensitivity is less significant. Referring to figure 6, we remark that the Keulegan-Carpenter number (KC) is very small for all of our results since the requirement that the motion is linear relies on the assumption that $A_I' \ll w'$, i.e., $KC/2\pi \ll 1$. From figure 5, we find that the

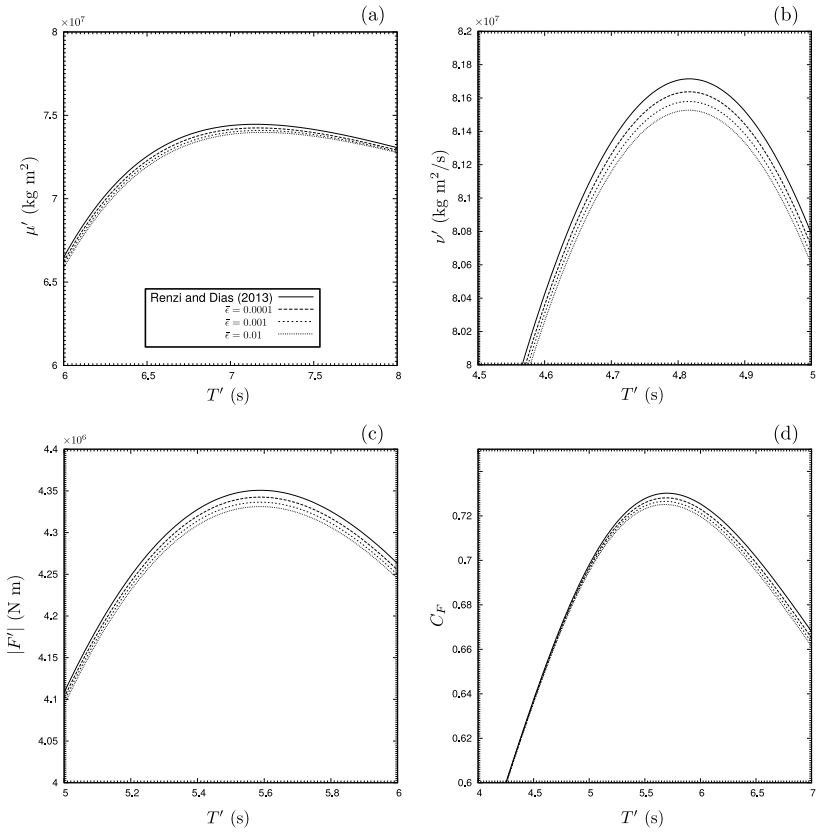

Fig. 4 The dependence of the peak values of each of the hydrodynamic coefficients (a)-(c) and the capture factor (d) as indicated in figure 3.

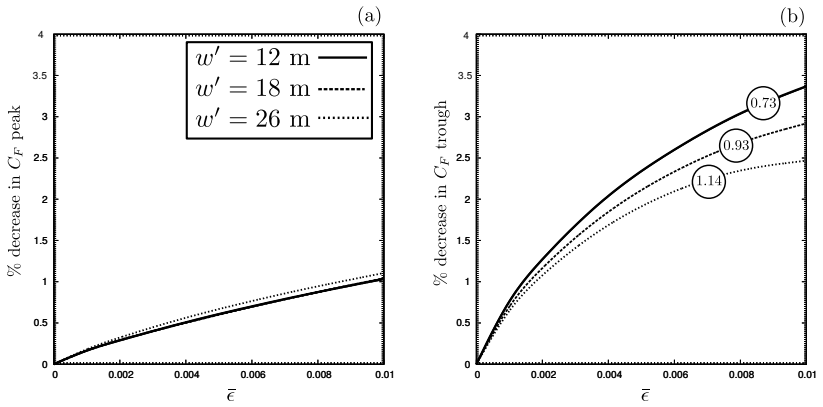

Fig. 5 The percentage decrease in the peak (a) and trough (b) values of the capture factor C_F versus the magnitude of the dissipation-effect parameter $\bar{\epsilon}$ for three flap widths $w' = 12, 18$, and 26 m. The numbers labelling the curves in (b) correspond to the diffraction parameter Kl for that curve.

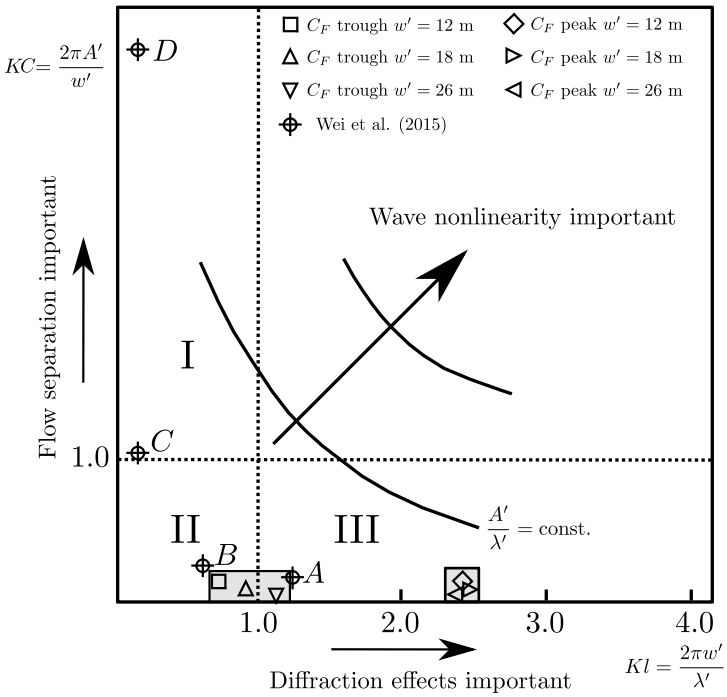

Fig. 6 The regions of validity of the hydrodynamic approximations (redrawn from [10]) in the Kl-KC parameter space. The CFD modelling carried out in [10] is indicated by the crosshairs, and each of the test cases are labelled A-D accordingly. The data from the parametric analysis (i.e., figure 5) is indicated by squares, diamonds, and triangles as shown.

relative importance of flow separation to diffraction effects is greater at longer wave periods (i.e., trough rather than peak values), and for narrower flaps. Hence, the hydrodynamic quantities are not sensitive to increasing dissipation effects when either the flap is very wide or the wave period short, in qualitative agreement with the conclusions of [10].

3.3 Influence of dissipation on flap in resonance with incident waves

If the flap is designed such that its buoyancy torque C and inertia torque I satisfy the relation

$$\omega^2(I + \mu) = C, \tag{67}$$

i.e., the flap is tuned to resonate with the incident waves, then it follows from (48) that $\nu_{\text{pto}} = \nu$ and the capture factor attains its maximal value

$$C_F^{\max} = \frac{|F|^2}{4A_I^2 C_g \nu}. \tag{68}$$

In this last subsection, we examine the case of a flap tuned to resonate with the incoming waves. To facilitate this study, we consider a narrow flap ($w' = 3$

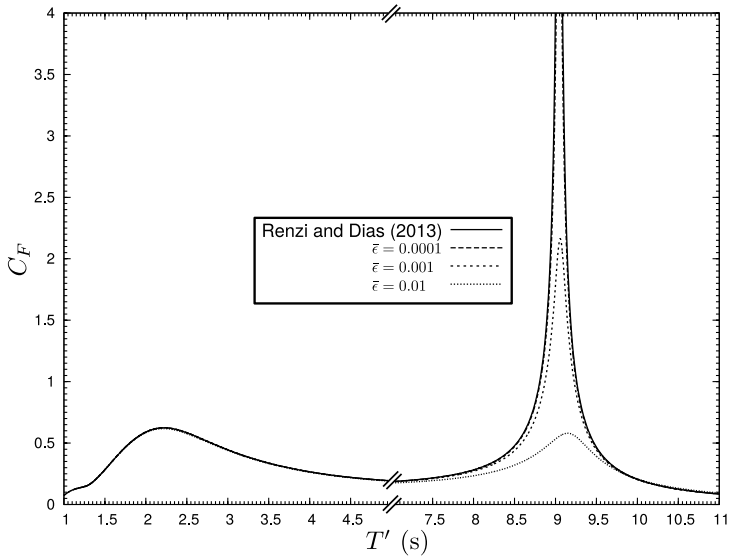

Fig. 7 The influence of dissipation on the capture factor of a 3 m wide flap tuned to resonance; the solid curve is calculated using the model of [5], and contains a spike at the resonant wave period at $T' \approx 9.04$ s, and the dissipative effect parameter $\bar{\epsilon}$ is increased from 0.0001 to 0.01 – note the broken horizontal axis at $T' = 5$ s.

m wide), which has a resonant period within the range of periods considered in this paper. Using the model formulated in [5], we find that the capture factor curve contains a spike near the flap's resonant period; however, including dissipation in the form of a pressure discharge near the flap's tips removes this spike. Referring to figure 7, we see that the capture factor has two peaks: one corresponding to the maximum in the wave torque (at $T' = 2.22$ s) and a second peak that spikes at the resonant period (at $T' = 9.04$ s). Figure 7 reveals the effect that increasing dissipation has on the resonant peak. We find that increasing $\bar{\epsilon}$ to 0.01 is sufficient to reduce the resonant peak to below the level of the peak corresponding to maximum exciting torque.

In figure 8, we explore the effect that dissipation has on the dynamics of the flap. Figure 8(a) shows an expanded view of C_F near the resonant period, while figure 8(b) shows the corresponding amplitude of rotation of the flap in dimensional variables. Near resonance, the inviscid theory predicts unrealistically large amplitudes of rotation. For $\bar{\epsilon}$ between 0 and 0.001, the predicted amplitude of rotation is still above 90°, however as $\bar{\epsilon}$ is increased further, we find that the flap's rotation amplitude near resonance rapidly decreases to $\Theta' \approx 33°$, which is accompanied by a shift in the resonant peak towards longer periods. Although this angle is a dramatic reduction on the value attained in the non-dissipative case, we remark that the linearised theory used here is unlikely to capture the dynamics of the flap at larger angles than this.

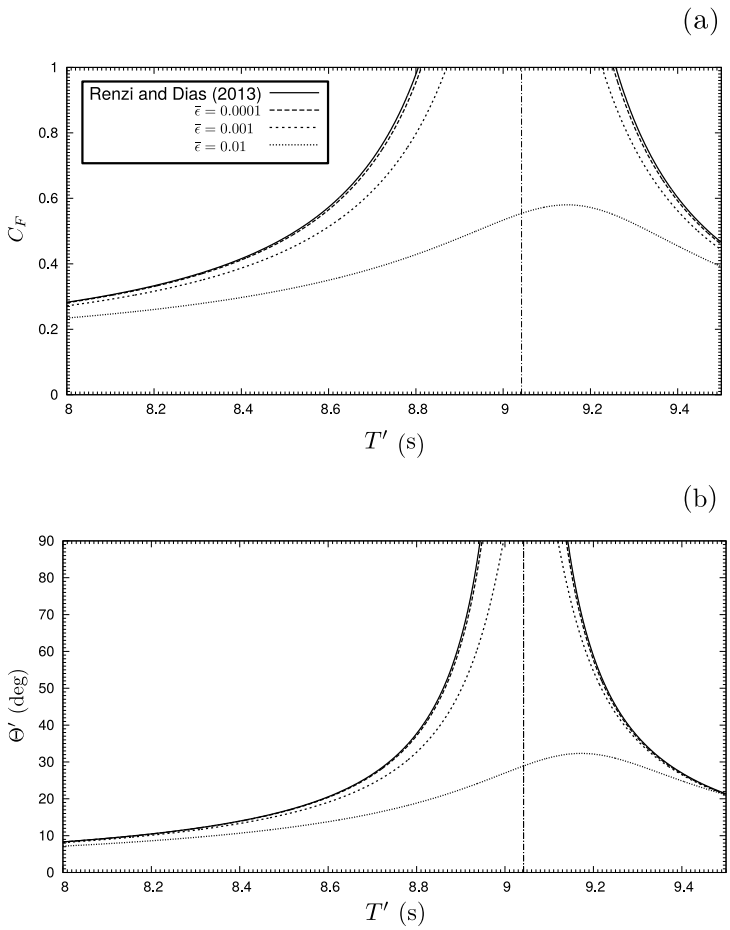

Fig. 8 The influence of dissipation on (a) the capture factor and (b) the amplitude of rotation of a 3 m wide flap. The solid curve is calculated using the model of [5], and contains a spike at the resonant wave period at $T' \approx 9.04$ s, and the dissipative effect parameter $\bar{\epsilon}$ is increased from 0.0001 to 0.01.

4 Discussion

It is well known that inviscid linear potential flow theory can greatly overpredict the dynamics of resonant systems, and that the addition of dissipation in regions where vortex-shedding is known to occur can give much better agreement with model tests [25]. The results presented here show that the effects due to vortex-shedding around a flap-type OWSC may be modelled by incorporating a pressure-discharge in the fluid surrounding the flap's tips. Furthermore, this approach has been shown to be an effective way to remove the spurious resonant behaviour of the flap as predicted by the inviscid theory.

One of the main results of this paper is the dependence of the capture factor C_F on the magnitude of the dissipative effect parameter $\bar{\epsilon}$: figure 3(d)

and figure 4(d). It shows that as $\bar{\epsilon}$ is increased, the capture factor decreases; it also shows that the dependence of C_F on $\bar{\epsilon}$ is most significant about the curve's peak and for long-period waves. Conversely, over the range of values considered for $\bar{\epsilon}$, on average, there is little dependence of C_F on $\bar{\epsilon}$ for typical environmental conditions experienced by an OWSC.

The parametric analysis involving different flap widths in figure 5 reveals that the trough values of the capture factor are more sensitive to changes in $\bar{\epsilon}$ than are the peak values. Moreover, this sensitivity is amplified as the flap is narrowed. This suggests that viscous effects will be less important for flaps with large Kl (i.e., wide flaps and/or short waves) and/or small KC numbers. In order to compare these results with existing data from CFD modelling, we represent the cases considered in the parametric analysis in figure 6, which is redrawn from [10]. In [10], viscous effects become more important as one shifts from region III (viscous effects are negligible) to region II, and then to region I (viscous effects dominate). Referring to our results (i.e., figure 5), we can see that the parametric study for short-period waves (large Kl) is far into region III (where there is little sensitivity to viscous dissipation), whereas the study in long-period waves is on the boundary between regions II and III (where the sensitivity to viscous dissipation is amplified). This amplification of the sensitivity at small Kl numbers and/or larger KC numbers is therefore in qualitative agreement with the conclusions in [10].

We have examined the case where the OWSC is tuned to resonate with the incoming waves. It is well known that using inviscid linear potential theory to capture resonant effects can lead to unphysical spikes in the hydrodynamic quantities. We find that an OWSC's capture factor exhibits this same behaviour using standard inviscid linear potential theory, but that the inclusion of dissipation in the form of a pressure discharge in the vicinity of the flap's tips is sufficient to eliminate this spurious behaviour. Although such wave conditions are not typically experienced for existing OWSCs, we have demonstrated that adding viscous dissipation in this way can smooth the spike in the capture factor and give a more realistic prediction of the hydrodynamic performance of the OWSC.

Moreover, we may determine the dissipative-effect parameter by comparing our predicted amplitudes of rotation (figure 8b) to data from laboratory tests and/or CFD simulations. The former methodology was used successfully in [13] to examine the effect of viscous dissipation on moonpool resonance and in [23] to calculate the resistive forces and wave loads on a porous plate. We remark that such a comparison would need to be conducted at wave periods close to the flap's resonant period (see [13]), where the most dramatic excursions in rotation amplitude occur.

5 Conclusion

We have examined the effect of viscous dissipation on the performance of an OWSC in the open ocean. Viscous effects are included in the region around

the flap's sharp edges, where vortex shedding is known to occur. The hydrodynamic modelling of the flap is based on linear potential flow theory, and the effects of viscous dissipation have been incorporated by assuming that there is a loss in hydrodynamic pressure, which is taken to be a function of the fluid's velocity in the direction normal to the flap, in the region surrounding the flap's edges. Using Green's theorem, this approach leads to a hypersingular integral equation for the velocity potential, in which the singularity is resolved by expressing the velocity potential in terms of a fast-converging series of Chebyshev polynomials.

We demonstrate that there exists a Haskind relation for the OWSC when dissipative effects are included, and we show that this relation is identical to the Haskind relation appearing in previous studies of an OWSC in the open ocean without viscous dissipation. In the dissipation-free case, it was found that evanescent modes do not contribute to the radiation damping. Therefore, it is interesting to point out that our Haskind relation holds even though the contribution of the $n > 0$ evanescent modes to the radiation damping are *non*-zero.

We show that the effects of dissipation are to reduce the peak values of the hydrodynamic quantities, and that the dependence of the hydrodynamic quantities on the dissipation-effect parameter is generally weak when considering the environmental conditions typically experienced by existing OWSCs. The effects of dissipation are strongest near peaks in the hydrodynamic quantities and for long-period waves. Conversely, the effect of dissipation is negligible for short-period waves. The capture factor, which is a measure of the OWSC's ability to extract energy from the ocean's waves, is reduced for increasing dissipation levels. The effect is weak across typical environmental conditions, with a reduction of about 1% and 3% in the peak and trough values of the C_F curve for an 18 m wide flap respectively as the dissipation-effect parameter is increased from 0.0001 to its maximum value of 0.01.

Our model is in qualitative agreement with existing CFD simulations and available experimental data, where previous authors have concluded that viscous drag is more important for narrow flaps and that the effects are amplified for long-period waves. We have thus validated the visco-potential approach for an OWSC in the open ocean, and have shown that it is an efficient and effective method to investigate the effects of dissipation on the flap's hydrodynamic performance in a range of environmental conditions. In addition, our analysis of a resonant OWSC shows that the spikes in C_F predicted by the inviscid theory may be removed by including dissipation in the model in the form of a pressure drop near the flap's tips.

This paper is primarily concerned with a single flap in the open ocean, and we find that the performance of the flap is largely insensitive to the magnitude of the dissipative-effect parameter. Conversely, the effect of dissipation on the resonant peak of the capture factor curve is dramatic. Since this resonant period lies outside the typical operating conditions of an OWSC, it does not have an appreciable effect on the operating hydrodynamic performance of an OWSC. However, it is interesting to speculate how the hydrodynamic per-

formance is affected when there are 'near resonant' phenomena present such as those described in [4, 7]. In order to examine this, one could reformulate the problem using a channel Green's function. Finally, note that we use a linear law to relate the pressure discharge to the local fluid velocity, but that a quadratic or other form could have been used. The quadratic and linear laws may be related using the Lorentz principle of equivalent work as described in [26, 27, 11]: hence, we do not expect such a choice to significantly affect our conclusions. To test this, the original equations (1)-(4) and (7) could, in principle, be solved using a BEM solver – these studies are left for future work.

Appendix: Solution to the diffraction and radiation problems

In this section, we present the solution to the system of equations for the n^{th}-mode 2D spatial potentials $\varphi_n^{(R,D)}$ ((32), (36), (39), and (40)) by using Green's theorem in the fluid domain. The method we use is based on the same procedure as devised by [6]; to begin, we define the Green's function

$$G_n(x,y;\xi,\eta) = \frac{1}{4\mathrm{i}} H_0^{(1)}\left(\kappa_n \rho\right), \tag{69}$$

to be singular at $(x,y) = (\xi,\eta) \in \Sigma$ as the outgoing solution of the Helmholtz equation

$$(\nabla^2 + \kappa_n^2) G_n = 0; \quad G_n \to \frac{\log \rho}{2\pi} \text{ as } \rho \to 0, \tag{70}$$

where $\rho = \sqrt{(x-\xi)^2 + (y-\eta)^2}$, $(\xi,\eta) \in \Sigma$; here $H_0^{(1)}$ is the Hankel function of the first kind and the zeroth order. To reduce the amount of cumbersome algebra, let us label the dimensionless start and end of each boundary by (y_m^s, y_m^e) respectively, where $m = 1, 3$ correspond to the dissipative surfaces and $m = 2$ labels the flap.

Application of Green's theorem to $\varphi_n^{(R,D)}(x,y)$ and $G_n(x,y;\xi,\eta)$ in the domain Σ enclosed by a large circumference centred at the origin O and containing the flap and dissipative surfaces, and using (40) yields

$$\begin{Bmatrix} \varphi_n^R \\ \varphi_n^D \end{Bmatrix}(x,y) = \sum_{m=1}^{3} \int_{y_m^s}^{y_m^e} \begin{Bmatrix} \Delta\varphi_{nm}^R \\ \Delta\varphi_{nm}^D \end{Bmatrix}(\eta) G_{n,\xi}(x,y;\xi,\eta)|_{\xi=0} \mathrm{d}\eta. \tag{71}$$

Here, we define

$$\begin{Bmatrix} \Delta\varphi_{nm}^R \\ \Delta\varphi_{nm}^D \end{Bmatrix}(y) = \begin{Bmatrix} \varphi_n^R \\ \varphi_n^D \end{Bmatrix}(-0,y) - \begin{Bmatrix} \varphi_n^R \\ \varphi_n^D \end{Bmatrix}(+0,y), \quad y \in (y_m^s, y_m^e); \tag{72}$$

i.e., the first line is the jump in the n^{th} radiation potential across the m^{th} region when the OWSC is moving with the remaining regions fixed, and the second line is the solution to the diffraction problem, which is solved by keeping all regions held fixed in incident waves.

Differentiating (71) with respect to x, and evaluating the expression on the flap and dissipative surfaces leads to a hypersingular equation comprising contributions from each

one of the regions [6]; using (36) and (39) we find that $\Delta\varphi_{nm}^{(R,D)}$ satisfy the integral equations

$$\sum_{m=1}^{3}\frac{\kappa_n}{4\mathrm{i}}\fint_{y_m^s}^{y_m^e}\begin{Bmatrix}\Delta\varphi_{nm}^R\\ \Delta\varphi_{nm}^D\end{Bmatrix}(\eta)\frac{H_1^{(1)}(\kappa_n|y-\eta|)}{|y-\eta|}\mathrm{d}\eta = \begin{cases}\begin{Bmatrix}f_n\\ A_I q_n\end{Bmatrix} & y\in(y_2^s,y_2^e)\\ -\dfrac{\omega^2}{\mathrm{i}\bar{\epsilon}}\begin{Bmatrix}\Delta\varphi_{nm}^R\\ \Delta\varphi_{nm}^D\end{Bmatrix}(y) & y\in(y_{1,3}^s,y_{1,3}^e),\end{cases} \tag{73}$$

where $\fint$ is interpreted as the Hadamard finite-part integral [28]. In order to resolve the singularity, we follow the analysis of [6] and perform the following change of variables:

$$u_m = y_m^s + y_m^e,\quad \zeta = \frac{2\eta-u_m}{w_m},\quad \begin{Bmatrix}\Delta\varphi_{nm}^R\\ \Delta\varphi_{nm}^D\end{Bmatrix}(\eta) = \begin{Bmatrix}Q_{nm}\\ S_{nm}\end{Bmatrix}(\zeta), \tag{74a, b, c}$$

where $w_m = y_m^e - y_m^s$ is the dimensionless width of the m^{th} region, and define

$$v_m(y) = \frac{2y-u_m}{w_m},\quad y\in(y_\beta^s,y_\beta^e),\quad \beta=1,2,3. \tag{75}$$

Inserting the change of variables (74) and (75) into (73) yields

$$\begin{aligned}\frac{\kappa_n}{4\mathrm{i}}\fint_{-1}^{1}\begin{Bmatrix}Q_{n\beta}\\ S_{n\beta}\end{Bmatrix}(\zeta)\frac{H_1^{(1)}(\frac{1}{2}\kappa_n w_\beta|v_\beta(y)-\zeta|)}{|v_\beta(y)-\zeta|}\mathrm{d}\zeta&\\ +\sum_{\substack{\gamma=1\\ \gamma\neq\beta}}^{3}\frac{\kappa_n}{4\mathrm{i}}\int_{-1}^{1}\begin{Bmatrix}Q_{n\gamma}\\ S_{n\gamma}\end{Bmatrix}(\zeta)\frac{H_1^{(1)}(\frac{1}{2}\kappa_n w_\gamma|v_\gamma(y)-\zeta|)}{|v_\gamma(y)-\zeta|}\mathrm{d}\eta&\\ = \begin{cases}\begin{Bmatrix}f_n\\ A_I q_n\end{Bmatrix} & y\in(y_2^s,y_2^e)\\ -\dfrac{\omega^2}{\mathrm{i}\bar{\epsilon}}\begin{Bmatrix}Q_{n\beta}\\ S_{n\beta}\end{Bmatrix}(v_\beta(y)) & y\in(y_\beta^s,y_\beta^e),\ \beta=1,3.\end{cases}\end{aligned} \tag{76}$$

Let us now expand the unknown jumps Q_{nm}, S_{nm} in a series of Chebyshev polynomials

$$\begin{Bmatrix}Q_{nm}\\ S_{nm}\end{Bmatrix}(\zeta) = (1-\zeta^2)^{1/2}\sum_{p=0}^{\infty}\begin{Bmatrix}b_{nmp}\\ A_I a_{nmp}\end{Bmatrix}U_p(\zeta),\quad m=1,2,3. \tag{77}$$

Inserting this expansion into (76) and truncating the series at some finite integer $p = p_{\max}$, yields a set of equations for the unknown coefficients $b_{n\beta p}$ and $a_{n\beta p}$; the equations, which are lengthy, are omitted here in the interests of brevity. This set of equations is solved using a numerical collocation scheme similar to the one devised in [6].

Acknowledgements This publication resulted from research conducted with the financial support of Science Foundation Ireland under Grant Number SFI/10/IN.1/I2996, 'High-end computational modelling for wave energy systems', for which the authors wish to express their gratitude.

References

1. Renzi E, Doherty K, Henry A, Dias F (2014) How does Oyster work? The simple interpretation of Oyster mathematics. Eur J Mech B/Fluids 47:124–131
2. Whittaker T, Folley M (2012) Nearshore oscillating wave surge converters and the development of Oyster. Phil Trans R Soc Lond *A* 370(1959):345–364
3. Falnes J (2002) Ocean Waves and Oscillating Systems. Cambridge University Press
4. Renzi E, Dias F (2012) Resonant behaviour of an oscillating wave energy converter in a channel. J Fluid Mech 701:482–510
5. Renzi E, Dias F (2013) Hydrodynamics of the oscillating wave surge converter in the open ocean. Eur J Mech B/Fluids 41:1–10, ISSN 0997-7546
6. Renzi E, Abdolali A, Bellotti G, Dias F (2013) Wave-power absorption from a finite array of oscillating wave surge converters. Renew Energ 63:55–68
7. Sarkar D, Renzi E, Dias F (2014) Wave farm modelling of oscillating wave surge converters. Proc R Soc Lond *A* 470(2167):20140118
8. Noad I, Porter R (2015) Optimisation of arrays of flap-type oscillating wave surge converters. Appl Ocean Res 50:237–253, ISSN 0141-1187
9. Sarkar D, Contal E, Vayatis N, Dias F (2016) Prediction and optimization of wave energy converter arrays using a machine learning approach. Renew Energ 97:504–517
10. Wei Y, Rafiee A, Henry A, Dias F (2015) Wave interaction with an oscillating wave surge converter, Part I: Viscous effects. Ocean Eng 104:185–203
11. van 't Hoff J (2009) Hydrodynamic modelling of the oscillating wave surge converter. Ph.D. thesis, Queen's University Belfast
12. Chakrabarti SK (2005) Chapter 4 - Loads and Responses. In SK Chakrabarti, editor, Handbook of Offshore Engineering, 133–196, Elsevier, London, ISBN 978-0-08-044381-2
13. Chen XB, Dias F, Duan WY (2011) Introduction of dissipation in potential flows. In Proc. 7th International Workshop on Ship Hydrodynamics*, Shanghai, China*
14. Tait M, El Damatty A, Isyumov N, Siddique M (2005) Numerical flow models to simulate tuned liquid dampers (TLD) with slat screens. J Fluid Struct 20(8):1007–1023
15. Tuck E (1975) Matching Problems Involving Flow through Small Holes, vol. 15 of *Advances in Applied Mechanics*. Elsevier
16. Evans D (1990) The use of porous screens as wave dampers in narrow wave tanks. J Eng Math 24(3):203–212
17. Yu X (1995) Diffraction of water waves by porous breakwaters. J Waterw Port Coast Ocean Eng 121(6):275–282
18. Molin B (2001) On the added mass and damping of periodic arrays of fully or partially porous disks. J Fluid Struct 15(2):275–290
19. Molin B, Remy F (2013) Experimental and numerical study of the sloshing motion in a rectangular tank with a perforated screen. J Fluid Struct 43:463–480
20. Terra GM, van de Berg WJ, Maas LR (2005) Experimental verification of Lorentz' linearization procedure for quadratic friction. Fluid Dyn Res 36(3):175–188
21. Folley M, Whittaker T, Van't Hoff J (2007) The design of small seabed-mounted bottom-hinged wave energy converters. In Proc. 7th European Wave and Tidal Energy Conf., Porto, Portugal, vol. 455
22. Folley M, Whittaker T (2010) Spectral modelling of wave energy converters. Coast Eng 57(10):892–897
23. Li Y, Liu Y, Teng B (2006) Porous effect parameter of thin permeable plates. Coast Eng J 48(04):309–336
24. Farley F (1982) Wave energy conversion by flexible resonant rafts. Appl Ocean Res 4(1):57–63
25. Chen XB, Liu HX, Duan WY (2015) Semi-analytical solutions to wave diffraction of cylindrical structures with a moonpool with a restricted entrance. J Eng Math 90:51–66
26. Sollitt CK, Cross RH (1972) Wave transmission through permeable breakwaters. In Proc. 13th Coastal Engng Conf., Vancouver, Canada, 1827–1846, ASCE
27. Mei CC (1989) The Applied Dynamics of Ocean Surface Waves. World Scientific
28. Linton CM, McIver P (2001) Handbook of Mathematical Techniques for Wave/Structure Interactions. CRC Press